A mechanism of spring Barents Sea ice effect on the extreme summer droughts in northeastern China

Yibo Du[1] · Jie Zhang[1] · Siwen Zhao[2] · Zhiheng Chen[1]

Abstract

The frequency of extreme drought events in northeastern China (NEC) has increased since the 2000s, and such a decadal anomalous trend may lead to significant stress on agriculture and economic development. The correlation between Arctic sea ice loss in spring and extreme summer droughts over NEC was investigated. The results show that the loss of sea ice over the Barents Sea in spring is associated with extreme droughts and positive height anomalies over NEC in summer. The physical processes include two pathways. First, sea ice loss from the Barents Sea to the Kara Sea results in reducing baroclinicity over the ice loss region but increasing baroclinicity over the ice melting region, which is favorable to the wave ridge over northern Europe and negative-phase Summer North Atlantic Oscillation (SNAO). One wave train originates from negative-phase SNAO over North Atlantic–Europe and spreads to central Europe, central Asia, and NEC. Second, another wave motion flux originates from the Barents–Kara Sea propagating eastward, and then disperses southward to NEC. Both wave trains lead to anomalous anticyclonic circulation and westward subtropical high, which favors descending motion and less water vapor flux, thereby contributing to extreme drought.

Keywords Arctic ice · Barents–Kara Sea · Extreme droughts

1 Introduction

Drought is characterized by below-normal precipitation, which has become an increasing concern in recent years. Under global warming conditions, severe drought events in northern China have occurred more frequently (Zhang et al. 2019), and they can significantly damage the development of society, economy, and agriculture. Since the 1980s, the frequency of severe droughts over northeastern China (NEC) and the duration of droughts have been increasing (Liang et al. 2011; Yu et al. 2014). These characteristics have expanded southward from the semiarid boundary of northern China in recent decades, and the grassland region of NEC has been decreasing at 2.8% per year (Ma and Fu 2006). In 2016, NEC suffered a severe drought in summer, leading to an economic loss of 15 billion yuan (Li et al. 2018). Moreover, the frequency and duration of extreme drought in NEC are increasing (Wang et al. 2016; Zhang et al. 2009). As NEC is an important economic region in northern China, the drought variation and causes of extreme drought should be studied.

From a water balance viewpoint, less precipitation can significantly affect drought occurrence (Yang et al. 2012) as it is directly linked with anomalous circulations. Previous research indicated that extreme droughts in NEC are dominantly influenced by the East Asian summer monsoon (Huang et al. 2007; Wu et al. 2009a, b). Weakened Asian monsoon can increase the drought frequency in NEC because of inadequate water vapor transport (Zhang and Zhou 2015), which leads to southern floods and northern droughts in east China.

Upon modulation of the monsoon circulation position, the positive-phase Pacific-Japan (PJ) pattern (Nitta 1987) exhibits an anticyclonic anomaly over northern China in drought years. In addition, the decadal variation of NEC precipitation

✉ Jie Zhang
zhangj@nuist.edu.cn

[1] Key Laboratory of Meteorological Disaster, Ministry of Education (KLME)/Joint International Research Laboratory of Climate and Environment Change (ILCEC)/Collaborative Innovation Center on Forecast and Evaluation of Meteorological Disasters (CIC-FEMD), Nanjing University of Information Science and Technology, Nanjing, China

[2] Institute of Atmospheric Environment, China Meteorological Administration (CMA), Shenyang 110166, China

is related to the phase shift of the Pacific Decadal Oscillation (PDO) (Han et al. 2015) because negative-phase PDO can reduce zonal sea-land thermal contrast, leading to positive water vapor transport anomalies. Furthermore, the interannual variation of precipitation over NEC is closely related to tropical sea surface temperature (SST) anomalies (Han et al. 2017; Sun and Wang 2012). For instance, the location and intensity of subtropical high are influenced by El Niño–Southern Oscillation (ENSO) (Wang et al. 2008), and Indian Ocean Dipole has impact on the meridional displacement of the East Asian jet in the boreal summer (Qu and Huang 2012).

Westerly circulations interact with monsoon circulations, thereby modulating the convergence region and water vapor flux, and contributing to extreme droughts and floods (Du et al. 2020; Zhang et al. 2018a, b). Previous studies suggest that droughts in NEC correspond to westerly anomalies and low-frequency waves (Zhang et al. 2020a, b). Since the twenty-first century, the mid-latitude wave train named the Silk Road Pattern has intensified, and it propagates along the Asian westerly jet in the upper troposphere, strengthening the meridional circulation of stationary wave and anticyclonic disturbance over NEC (Lu et al. 2002; Hong et al. 2017; Zhang et al. 2019). Upstream of such low-frequency waves, the Summer North Atlantic Oscillation (SNAO) has a smaller spatial extent and is located farther north. Du et al. (2020) studied the impact of the eastward shift in the negative-phase SNAO on extreme drought over northern China in summer. The SNAO experienced a pattern change after 2000 as the southern center started shifting eastward (Du et al. 2020; Zhang et al. 2020a, b). In addition, NAO is not only related to the internal dynamic process of the atmosphere, but also to external forces such as the El Niño–Southern Oscillation (Wu and Zhang 2015), North Atlantic SST (Kushnir et al. 2002; Pan 2005), and Arctic sea ice (Petoukhov and Semenov 2010; Wu et al. 2016).

Previous studies have revealed the potential effect of external factors on summer droughts over NEC, which are related to Atlantic Multidecadal Oscillation (AMO) (Zhang et al. 2020a, b), ENSO event (Dai 2013), and snow cover over Eurasia (Wu and Kirtman 2007), while few studies have focused on the influence of Arctic sea ice. In fact, the loss of Arctic sea ice is an important potential driver, and it can force mid-latitude climate changes over Eurasia (Guo et al. 2014; Li and Wang 2013). For example, Nakamura et al. (2019) has pointed out the cooling anomalies over the Eurasian continent is closely related to the land process induced by the loss of sea ice. Zhang et al. (2020a, b) have pointed out that the increase in European summer heat waves is closely linked to reduction of the spring Arctic sea ice via the excitation of the anomalous Eurasian wave train. Wu et al. (2016) have reported that the Arctic sea ice in Norwegian Sea and Barents Sea in the preceding winter

is intimately connected with interannual variations of East Asian spring precipitation. In addition, some studies have indicated that dipole rainfall pattern over eastern China in August associated with negative interannual variability of the sea ice over Barents–Kara Sea in July and August (Shen et al. 2019).

Since 2000, the Barents Sea has been one of the most dramatic regions of Arctic sea ice loss, with smaller sea ice covers in autumn. The reduced sea ice in the Barents–Kara Sea during autumn–winter is considered a driver of anomalous weather and climate over mid-latitude Eurasia (Petoukhov and Semenov 2010; Kim et al. 2014). Some studies mentioned that the decline in the Barents Sea ice can affect the Siberia High, which would strengthen the East Asian winter monsoon (Inoue et al. 2012; Wu et al. 1999). Tang et al. (2014) revealed that the reduction of Arctic sea ice may lead to decline in the meridional temperature gradient between polar and mid-latitude regions, and this decline could cause cold winter extremes in the northern hemisphere. Recently, He et al. (2017) observed that the decline of sea ice over the Barents Sea in June led to an anomalous rainfall pattern over eastern China through mid-latitude wave trains. Zhang et al. (2018a, b) observed that variations in the Ural blocking in summer displayed a statistically significant association with a persistent spring–summer sea ice pattern in the Barents–Kara Sea.

In addition to summer and autumn, Arctic sea ice loss is also significant in spring. However, there are few studies on the possible connections between spring sea ice and extreme summer climate events over China. Nevertheless, Li et al. (2018) observed that the sea ice loss over the Barents Sea in March might influence hot drought events over NEC in summer, with a significant causal relationship between them. Considering the Arctic sea ice loss in spring, this study aims to answer two issues. First, we aim to identify the correlation between the spring Barents Sea ice and extreme droughts in NEC and the related westerly circulation anomalies. Second, we aim to investigate the mechanism through which the spring Barents Sea ice affects extreme droughts over NEC in August. By exploring these two issues, we aim to enable the prediction of extreme drought events for disaster defense and ecological protection.

2 Data and methods

2.1 Datasets

Atmospheric circulation fields with horizontal resolution of $1° \times 1°$ were obtained from ERA-Interim reanalysis data (http://apps.ecmwf.int/datasets/). Monthly variables including geopotential height, zonal and meridional wind components, and mean sea level pressure were used.

Monthly Arctic sea ice concentration (SIC) datasets were obtained from the Hadley Centre, at a horizontal resolution of $1° \times 1°$ (Rayner et al. 2003). The monthly mean SST data with horizontal resolution of $2° \times 2°$ were based on the Extended Reconstruction SST version 5 (ERSST 5) dataset, which was available from the National Oceanic and Atmospheric Administration website (Smith and Reynolds 2003). The observation precipitation dataset, with a resolution of $2.5° \times 2.5°$, was obtained from the Global Precipitation Climatology Project (GPCP). The monthly mean NAO indices were acquired from the Climate Prediction Center website (ftp://ftp.cpc.ncep.noaa.gov/cwlinks).

The monthly self-calibrating Palmer drought severity index (sc-PDSI, Dai 2011a) is a meteorological drought index that considers both water supply and demand, and it reflects the soil moisture deficit or surplus. Moreover, the sc-PDSI index is more scientific and objective than the original PDSI because it calibrates the PDSI by using local coefficients (Dai 2011b). In addition, the Penman–Monteith method is used to calculate potential evapotranspiration, because it is considered to be the most physical based and reliable method. The sc-PDSI data with Penman–Monteith equation used in this study were obtained from the Climate Data Guide website (https://climatedataguide.ucar.edu/climate-data/palmer-drought-severity-index-pdsi) at a $2.5° \times 2.5°$ horizontal resolution. Moderate drought is sc-PDSI ≤ -2, severe drought is sc-PDSI ≤ -3, extreme drought is sc-PDSI ≤ -4. The extreme drought is defined as an sc-PDSI lower than -3 in this study.

The SIC index (SICI) is defined as the spatial-weighted SIC averaged in spring over the Barents Sea (70° N–77° N, 30° E–60° E). The underlying surface turns into seawater due to the loss of sea ice. Therefore, the BSSTI is defined as the spatial-weighted sea surface temperature in August over Barents Sea (70° N–77° N, 30° E–60° E). The KSSTI is calculated as the spatial-weighted sea surface temperature in August over Kara Sea (70° N–77° N, 65° E–90° E). The BKSSTI is the average of BSSTI and KSSTI in August.

2.2 Methods

The wave activity flux (TNF; Takaya and Nakamura 2001) was used to diagnose the horizontal wave propagation associated with a teleconnection pattern on a basic flow zonally varying in the middle–upper troposphere. Based on the Wentzel–Kramers–Brillouin (WKB) approximation, the flux is independent of wave phase and parallel to the local group velocity of stationary Rossby waves. The flux in the pressure (P) coordinate can be expressed as follows:

$$W = \frac{P}{2000|U|} \begin{cases} U\left(v'^2 - \Psi'v'_x\right) + V\left(-u'v' + \Psi'u'_x\right) \\ U\left(-u'v' + \Psi'u'_x\right) + V\left(u'^2 + \Psi'u'_y\right) \\ \frac{f_0 R_0}{N^2 H_0}\left[U\left(v'T' - \Psi'T'_x\right) + V\left(-u'T' - \Psi'T'_y\right)\right] \end{cases},$$

(1)

where u and v are the horizontal winds, Ψ' is the streamfunction, R_0 is the gas constant, N^2 is the buoyancy frequency (Brunt–Väisälä frequency), H_0 is the atmospheric scale height, and T is the temperature. In Eq. (1), the background field includes the zonal non-uniform base flow and meridional wind field. Therefore it is suitable for a mid–high latitude circulation field analysis.

The Eady growth rate (EGR) was calculated to determine the atmospheric baroclinicity (Zhang et al. 2018a, b) as shown in Eq. (2).

$$\sigma = 0.31 \frac{f}{N} \frac{du}{dz},$$

(2)

where f is the Coriolis parameter, N is the Brunt–Väisälä frequency, u is the zonal wind, and z is the height. The EGR at 700 hPa was calculated to clarify the atmospheric baroclinicity response to underlying surface variation.

The Mann–Kendall test is a non-parametric statistical test method, which can clarify the start time of the mutation. The two curves of UF and UB have an intersection point, and the intersection point is between the critical lines, then the time corresponding to the intersection point is mutation time. Statistical techniques employed in this study included correlation, composite, and regression analyses. The statistical significance tests were computed using the Student's two-tailed t test.

3 Results

3.1 Characteristics of Arctic sea ice from spring to summer and drought distribution in NEC

In this study, we focus on the transitional spring season, defined as MAM. In MAM (Fig. 1a), the Barents Sea is dominated by abundant sea ice, and the SIC in the north of Arctic exceeds 90%. From spring to summer, sea ice gradually melts eastward and northward from the Barents Sea (Fig. 1b–d). By June, the sea ice has melted, except for the northern part of the Barents Sea region, and it nearly disappears over the Kara Sea in August. The frequency of droughts (sc-PDSI ≤ -2) and extreme droughts (sc-PDSI ≤ -3) over NEC in 1979–2017 are shown in Fig. 1e, f. The value indicates a high frequency of droughts and extreme droughts over NEC. Extreme droughts are mostly located in the southern part of NEC. Figure 1g, h show the
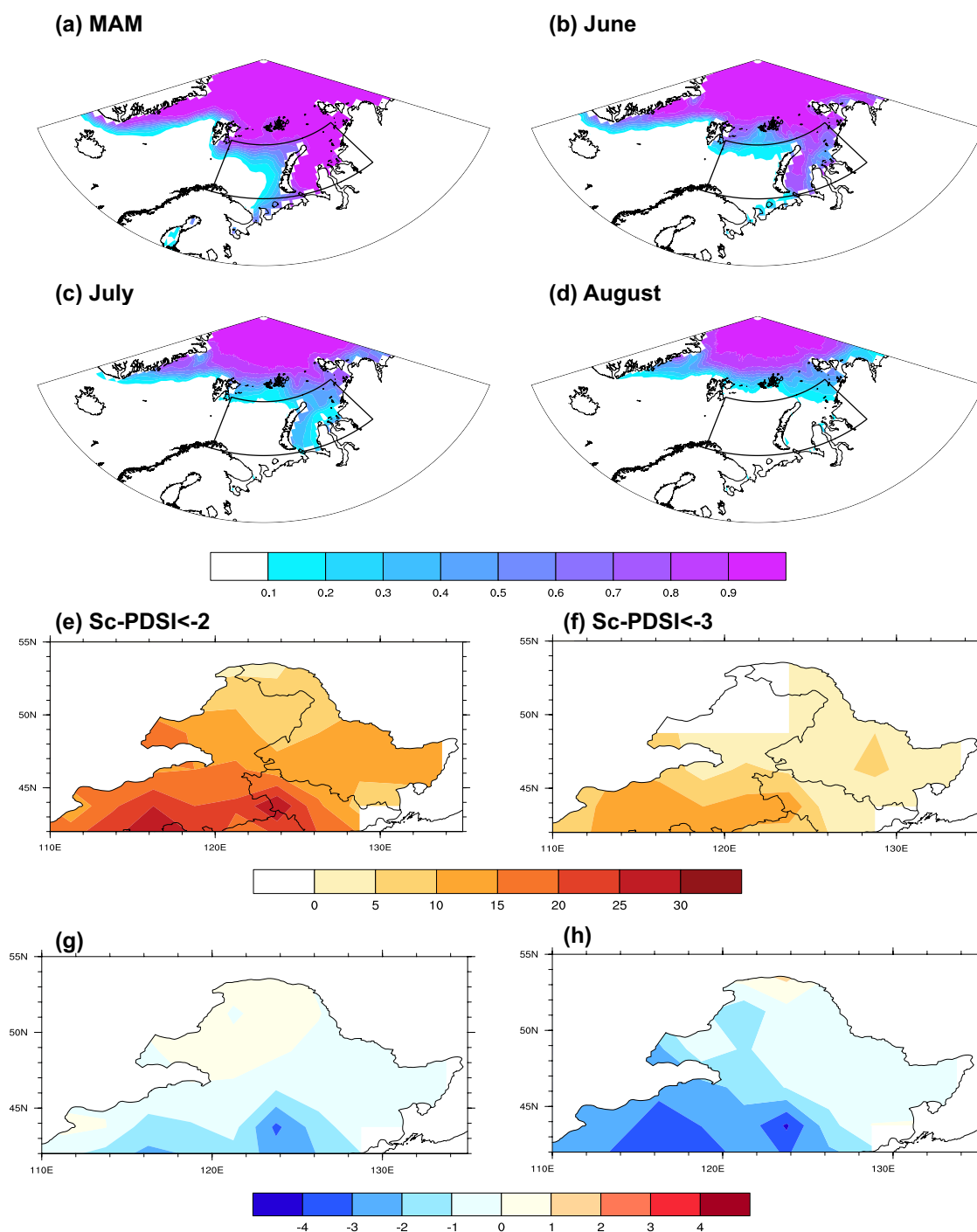
Fig. 1 Monthly climatological SIC in the Arctic region: **a** March to May (MAM), **b** June, **c** July, and **d** August (unit: %). Frequency of **e** droughts and **f** extreme droughts over NEC in August (unit: days). Drought spatial distribution over NEC in August: **g** 1979–1997 and **h** 1998–2017

drought spatial distribution characteristics in two periods, which were determined by the Mann–Kendall statistical test (Fig. 3b). Compared with the period from 1979–1997, the drought classification and affected areas clearly increased during 1998–2017.

Previous studies have discussed the relationship between autumn and winter Barents Sea ice and climate anomalies across East Asia (Fan et al. 2017; Wu et al. 1999). However, the variation of sea ice depends on the selected season. Therefore, it is necessary to identify the crucial sea ice areas

in spring. Figure 2a indicates the leading mode of the EOF for the spring sea ice anomalies over the Arctic, and the variance of this leading mode is 34.3%. The EOF mode clearly reflects the variation of spring sea ice over the Arctic region, and there is a considerable negative sea ice center over the Barents Sea, indicating that the variation of spring sea ice is more sensitive in the Barents Sea than in other regions. The PC1 shifted to a predominantly positive anomaly after 1990, indicating that the spring Barents Sea ice decreased remarkably during this period. Figure 2b displays the time series of SICI (red line) in spring from 1979 to 2017, which shows a decreased trend. The correlation between PC1 and SICI was significant, at − 0.96, indicating that the Barents Sea ice is more representative in the Barents Sea than in other Arctic areas.

3.2 Relationship between Barents Sea ice and droughts over NEC

Despite the known high temperatures and serious precipitation deficiencies over NEC 2016, these events might not occur with extreme droughts, and temperatures and precipitation cannot fully indicate the classification of drought. In order to better illustrated the characteristics of drought over NEC, we employ the meteorological drought index sc-PDSI. As shown in Fig. 3a, the time series of the sc-PDSI over NEC in August (42° N–50° N, 110° E–130° E) showed interdecadal variation at around 1998 based on the 9-year moving average. The trend of drought over NEC intensified in 1979–2017, and extreme drought events (sc-PDSI ≤ − 3) occurred ten times from 1979 to 2017. Extreme drought events occurred eight times after 1998. Figure 3b shows the Mann–Kendall test of sc-PDSI, and

it is clearly that the significant abrupt points of decadal changes of sc-PDSI began in 1998. The abrupt time point of the sc-PDSI was consistent with the results based on the 9-year moving average. Figure 3c displays the standardized values of SICI and sc-PDSI over NEC from 1979 to 2017, and their variations are more in phase after 1998. Li et al. (2018) have shown that the Barents Sea ice in March was significantly correlated with severe hot drought events over NEC after 1997, and this time point is also consistent with the time period when the frequency of extreme drought events increased. We calculated the correlation coefficients between SICI and sc-PDSI, and correlation coefficient (0.58) was obtained for 1998–2017 which is significant at the 95% confidence level, indicating that drought events are more likely to occur when the loss of Barents Sea ice occurs in spring.

To document the spatial distribution of the correlation during two periods, Fig. 4a, b show the correlation between SICI and sc-PDSI over NEC. It is clearly that sc-PDSI anomalies over NEC display a strong positive correlation with SICI after 1998, but there was no significant correlation over NEC for 1979–1996. In this latter period, the correlation between the sc-PDSI of NEC and the Barents Sea ice was significant, and there were positive correlation coefficients over the Barents Sea. In contrast, few areas over the Barents Sea were related to the sc-PDSI of NEC in 1979–1996.

As described above, the drought events over NEC in summer were closely related to the loss of spring sea ice over the Barents Sea. In this context, the mechanisms through which the Barents Sea ice affects the extreme drought events over NEC in summer are still unclear. It was worth discussing the mechanisms of the Barents Sea ice affecting the extreme drought over NEC.
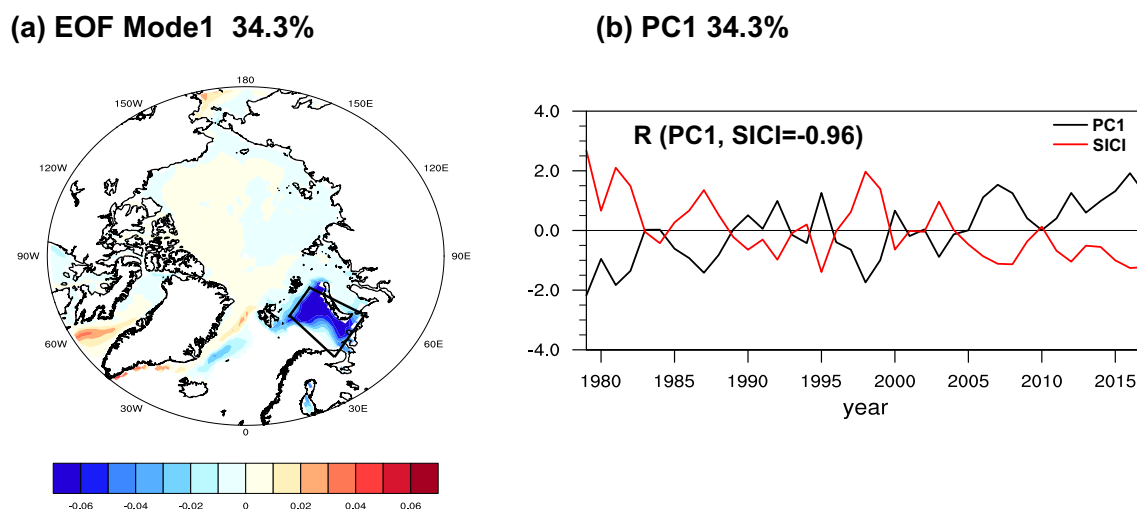
(a) EOF Mode1 34.3%

(b) PC1 34.3%

Fig. 2 **a** Leading mode of EOF for the Arctic Sea ice in MAM, and **b** normalized leading principal component (black line) and SIC index over the Barents Sea [red line: SIC index (SICI)]. Units are arbitrary
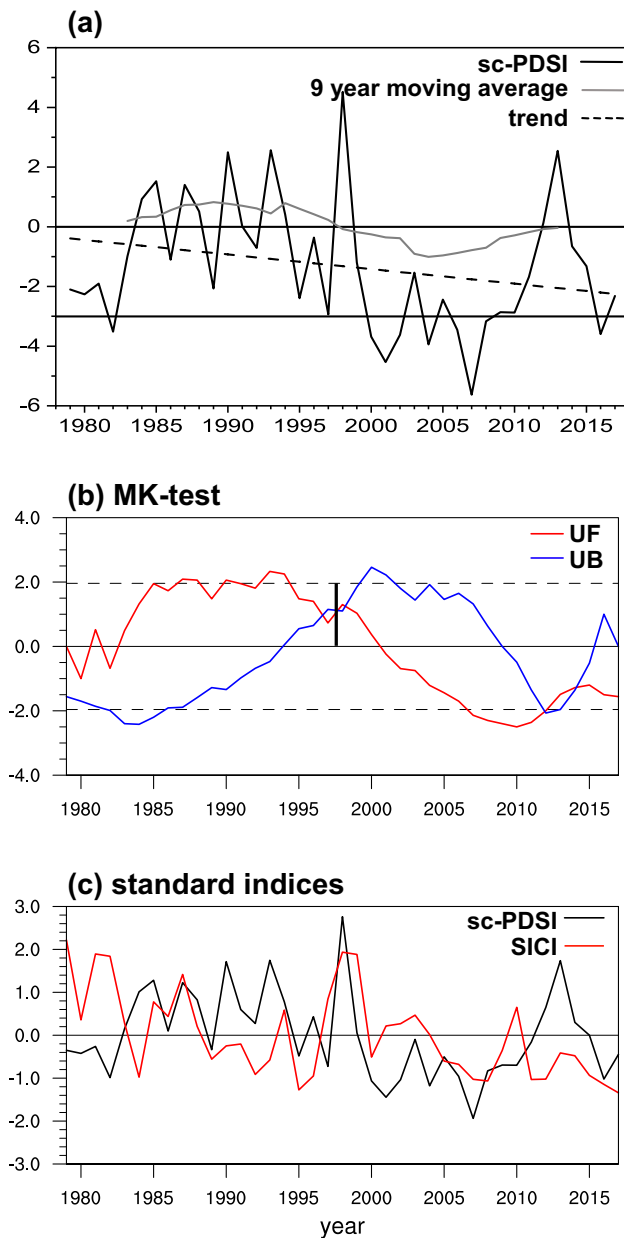
(a)

(b) MK-test

(c) standard indices

Fig. 3 **a** Time series of sc-PDSI over NEC in August from 1979 to 2017, **b** Mann–Kendall statistic test of sc-PDSI, and **c** time series of standardize sc-PDSI over NEC (black line) and SICI (red line) from 1979 to 2017. The gray line in **a** is the 9-year moving average of standardized sc-PDSI

3.3 The mechanisms of the Barents Sea ice affecting the extreme drought

3.3.1 Response of atmospheric circulation anomaly with reduced spring sea ice

To provide more details on the regional climate change related to the spring sea ice anomaly over the Barents Sea, regression maps of SIC, albedo (AL), net shortwave radiation (SW), and Eady growth rate (EGR) with regards to inverted SICI are shown in Fig. 5a–e. A reduction in the spring sea ice over the Barents Sea (Fig. 5a) led to fewer surface albedo anomalies over the Barents Sea and surrounding areas, including the Kara Sea (Fig. 5c), indicating the possibility of more absorption of incoming shortwave flux (Fig. 5d). This shows that the net shortwave radiation over the Barents Sea increases and accelerates the melting of the sea ice in spring. Sea ice changes the radiation state of the ocean surface through albedo feedback, leading to anomalies in the thermodynamic conditions of the sea surface and ocean–atmosphere heat exchange (Deser and Teng 2008; Dethloff et al. 2006). Therefore, there is an increase in the EGR over the Barents Sea and its surroundings due to the melting of sea ice (Fig. 5e). Meanwhile, the underlying conditions change from sea ice to seawater, resulting in enhanced atmospheric baroclinicity. In addition, spring snow depth over Eurasian is significantly correlated with sea ice over Barents Sea, and the increased baroclinicity in the southern land of the Barents and Kara seas may be related to the decrease in Eurasian spring snow cover (Fan et al. 2017; Li et al. 2018). As the melting continues, the sea ice over the Barents and Kara seas become even smaller in subsequent months, leading to a broad area of seawater (Fig. 5b). Thus, we focused on the regression map of SW, EGR, sea level pressure (SLP), and horizontal wind in June with regards to the SST over Barents Sea in June. Figure 5d shows the atmospheric circulation anomalies related to the loss of sea ice. A negative SLP center can be observed over the Barents Sea, and low surface pressures were attributed to the reduction of Barents Sea ice, with higher SST. The loss of sea ice decreases cold air accumulation and increases temperature in the lower troposphere, which could reduce the SLP (Zhang et al. 2015). Previous studies have also reported that numerical experiments can simulate the low-pressure structure in SLP resulting from sea ice loss (Blüthgen et al. 2012).In June, the anomalous southwesterly wind blows to the Kara Sea under the influence of low-level wind fields, leading to warm air from south and warm seawater from Barents Sea to accelerate the melting of sea ice in Kara Sea (Fig. 5f). Therefore, the melting of sea ice in the Kara Sea corresponds to increased baroclinicity of atmosphere (Fig. 5h). Due to the underlying surface of Barents Sea has turned into seawater in June, and the underlying surface did not change from June to August resulting in decreased baroclinicity of atmosphere.

As described above, the decreased sea ice causes anomalies in regional atmospheric signals, which are linked to surface state dependence. Previous studies have reported that the amplitude of the regional geopotential height field is influenced by the Arctic Sea ice loss, and this influence depends on the change of pre-existing surface state conditions (Overland et al. 2016; Shepherd 2014). To determine the response of the atmosphere to the loss of sea ice in the
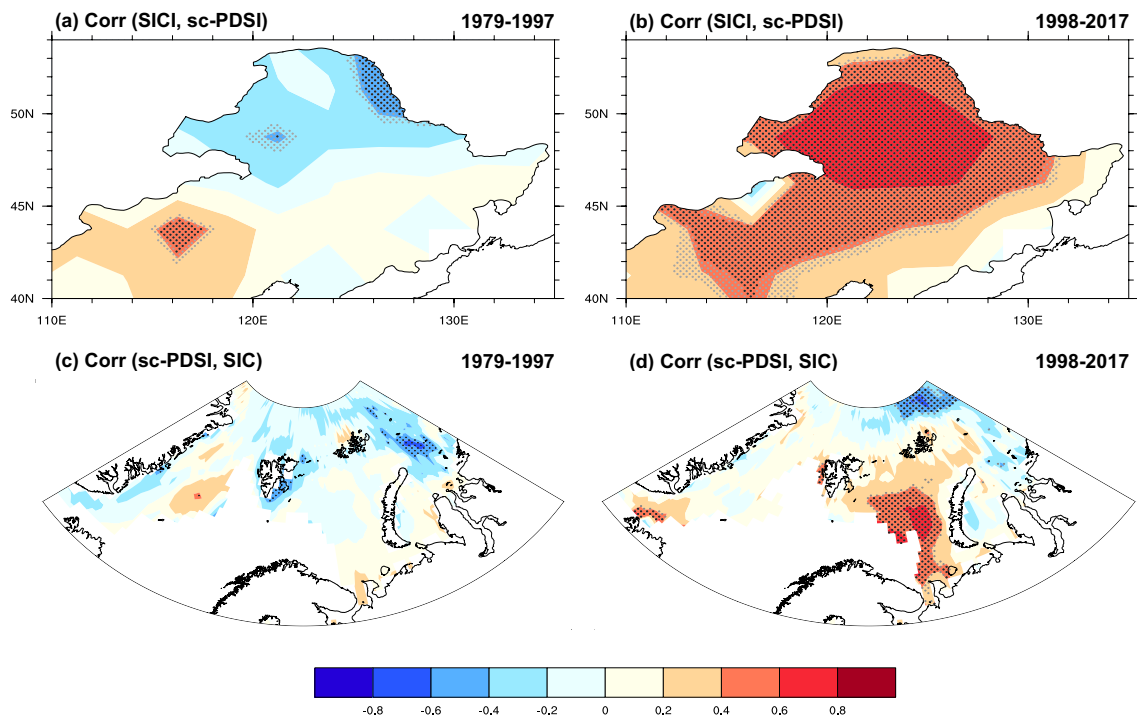
Fig. 4 Correlation between SICI and sc-PDSI over NEC in **a** 1979–1996 and **b** 1998–2017. Correlation between sc-PDSI of NEC and SIC over the Arctic in **c** 1979–1996 and **d** 1998–2017. Gray and black dots indicate significant correlations at the 90 and 95% confidence levels

following months, typical low sea ice years were selected based on a standardized SICI of less than -0.5 in order to obtain more samples. Therefore, the years with low sea ice were 2000, 2006, 2007, 2008, 2011, 2012, 2013, 2014, 2015, 2016 and 2017. Figure 6 presents monthly composite mean anomalies of geopotential height at 500 hPa from June to August. For low sea ice years, the negative geopotential height over Barents Sea moves eastward to Kara Sea. In summer, the melted Barents Sea ice reduces the meridional temperature gradient between the Barents Sea and Europe, and the lower atmosphere baroclinicity over the Barents Sea could cause Greenland high to expand southeast, leading to anomalous block circulation. Therefore, anomalous positive geopotential height forms over Europe in July and August, and the upstream areas depict the characteristics of negative-phase SNAO with the southern center shifting eastward in summer (Fig. 6b, c). In fact, the anomalous positive geopotential height forms over Europe could strengthen the climatological ridge, which also strengthen the climatological trough in the upstream via downstream influence. Therefore, the anomalous cyclonic over the southern center of SNAO pattern is enhanced due to the strengthening of climatological trough. Meanwhile, the anomalous positive geopotential forms over Greenland in low sea ice years, and the positive geopotential height over Greenland and the negative geopotential height over Europe–North Atlantic region are SNAO pattern. Hence, the enhanced northern

activity center of SNAO pattern also lead to the enhanced southern activity center of SNAO pattern. This configuration reveals the strengthening of climatological ridge and trough, which could enhance meridional circulation and low-frequency waves. Therefore, anticyclone anomalies would occur in August over NEC. The change in surface properties (albedo, surface net shortwave radiation, etc.) enhances the atmospheric baroclinicity due to reduced sea ice, and following the initial baroclinic stage of adjustment, the response becomes barotropic and amplified in space and magnitude. The adjustment balance is reached a few months later, and is characterized by a barotropic structure resembling the NAO pattern (Deser et al. 2000, 2007; Ferreira and Frankignoul 2005). A few previous studies also indicate that negative sea ice anomalies have a strong impact on atmospheric circulation (Alexander et al. 2004; Wang and Overland. 2009; Ogi et al. 2010; Mori et al. 2014).

In recent studies, Du et al. (2020) and Wang et al. (2018) demonstrated that the negative-phase of the SNAO may be a driver of extreme events in northern China, implying that the upstream SNAO may be crucial for the occurrence of extreme drought over NEC. Figure 7a shows the leading mode of the EOF for geopotential height anomalies at 500 hPa in August, with a variance of 24.4%. The EOF mode shows a clear positive and negative anomaly pattern from north to south, similar to the distribution of the geopotential height anomalies over the North Atlantic–Europe region
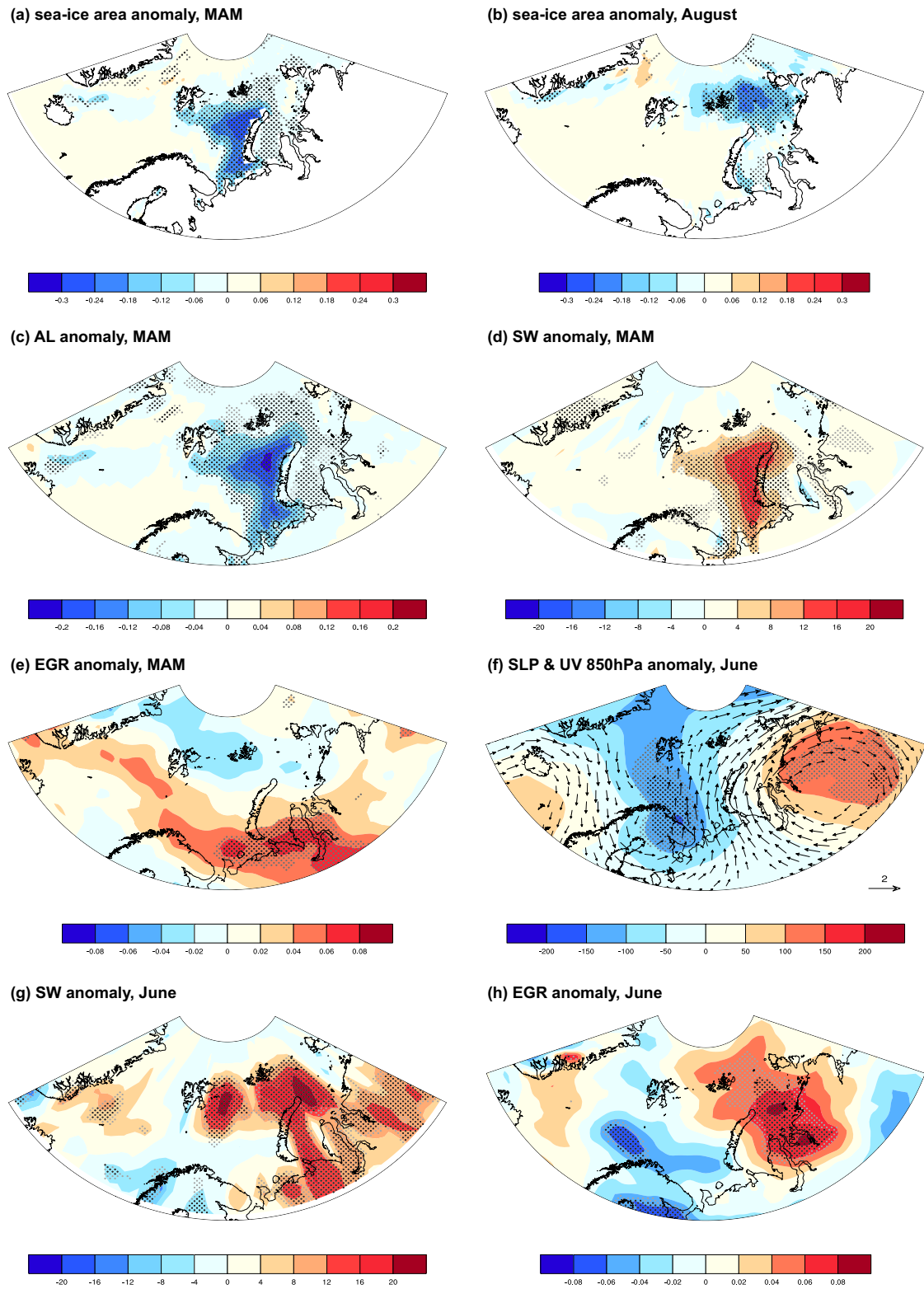
(a) sea-ice area anomaly, MAM

(b) sea-ice area anomaly, August

(c) AL anomaly, MAM

(d) SW anomaly, MAM

(e) EGR anomaly, MAM

(f) SLP & UV 850hPa anomaly, June

(g) SW anomaly, June

(h) EGR anomaly, June

Fig. 5 Regression map of sea ice concentration (MAM) with regard to **a** inverted SICI over Barents Sea in 1998–2017, **b** sea ice concentration (SIC) in August, **c** surface albedo (%), **d** surface net shortwave radiation (W/m^2), and **e** Eady growth rate (day^{-1}). Regression map of sea level pressure (Pa) and horizontal wind (m/s; vectors) at 850 hPa (**f**) with regards to SST over Barents Sea in June; **g** net shortwave radiation at surface (W/m^2), and **h** Eady growth rate (day^{-1}). Gray and black dots indicate significant regression coefficients at the 90 and 95% confidence levels

Fig. 6 Composite differences of geopotential height (gpm; shaded) at 500 hPa (1998–2017) between the low sea ice years and the climatology in **a** June, **b** July, and **c** August. Green and red contours represent averaged geopotential height of 5500–5700 gpm before and after 1998, respectively, with an interval of 50 gpm
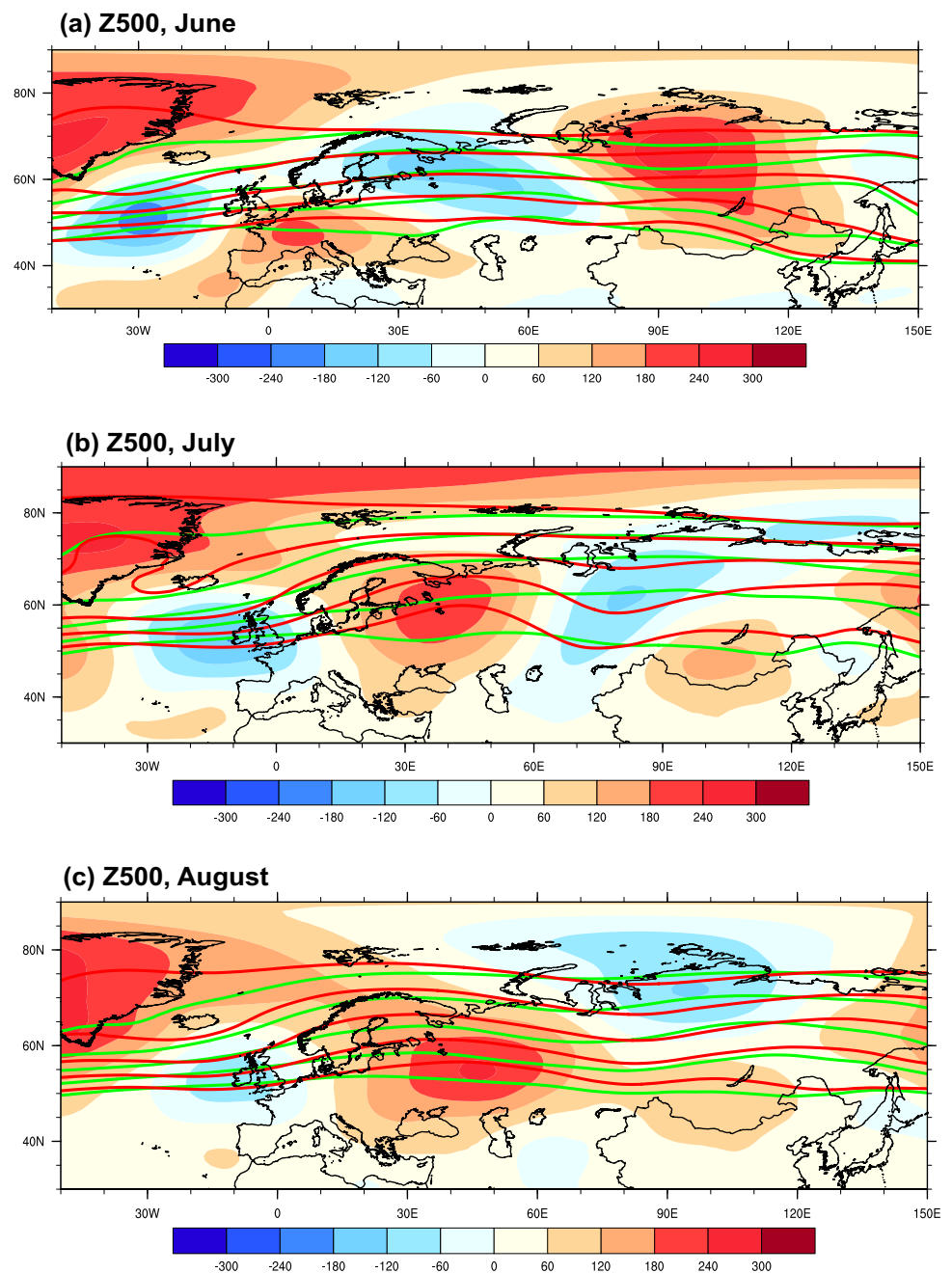
(Fig. 6c). The latitudinal pattern of the geopotential height anomaly indicates an eastward shift of the SNAO pattern due to a low-pressure anomaly over the west coast of Europe. As shown in Fig. 7b, PC1 changed from negative to positive at around 2000, which corresponded to the phase shift of SNAO. Additionally, PC1 presented a significant correlation of − 0.7 with SNAO at the 99% confidence level.

In August, the negative-phase SNAO with the southern center shifting eastward over North Atlantic region, and the sea ice melts into seawater over Barents–Kara Sea. The correlation coefficients between BSSTI, KSSTI, BKSSTI, SICI, SNAO, and PC1 in July and August of 1998–2017 are presented in Table 1. We confirmed that the August SNAO index was highly correlated with the SICI, and their correlation coefficients exceeded 0.5. Meanwhile, the correlation between the SNAO index and KSSTI and BKSSIT were also significant, which indicates that the underlying surface variation of the sea ice melting could affect the SNAO phase. However, the correlation between the SNAO index and BSSTI was not significant likely because the Barents Sea ice mostly melts in June (Fig. 1b). Additionally, the underlying surface over the Barents Sea is the seawater from June to August, whereas the SST evolution
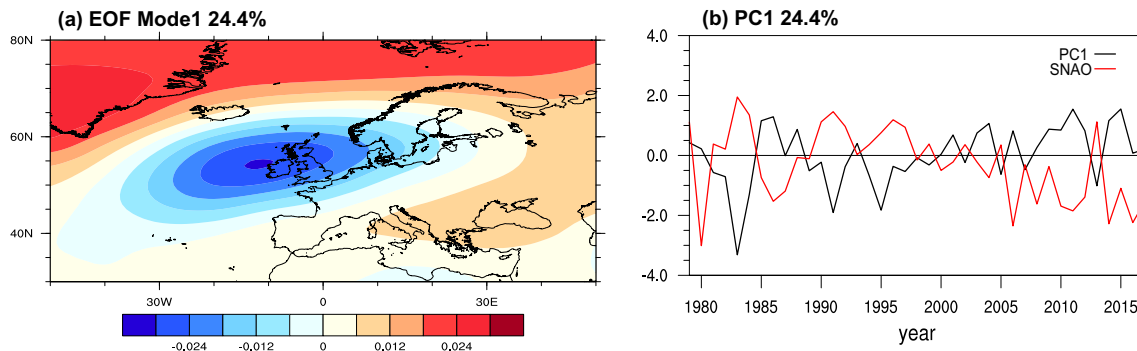
Fig. 7 a Leading mode of EOF for geopotential height at 500 hPa in August, and **b** normalized leading principal component (black line). The units are arbitrary. The red line is the standardize SNAO index

Table 1 Correlation coefficients between Barents SST index (BSSTI), Kara SST index (KSSTI), Barents–Kara SST index (BKSSTI), SICI, SNAO, and PC1 in July and August

	July PC1	July SNAO	August PC1	August SNAO
MAM SICI	− 0.21	0.2	− 0.24	0.51**
BSSTI	0.16	− 0.22	0.18	− 0.25
KSSTI			0.37*	− 0.41*
BKSSTI			0.28	− 0.38*

Double asterisks and single asterisks indicate correlation coefficients that exceed the 95 and 90% confidence levels, respectively
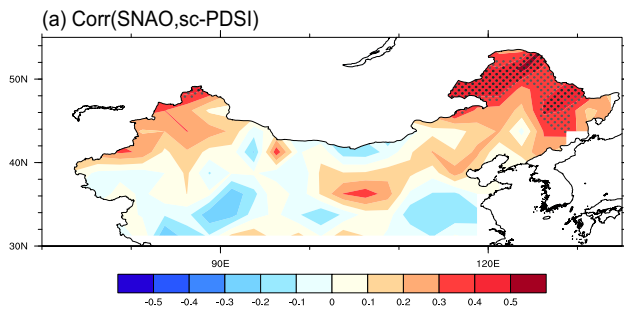

Fig. 8 Correlation between SNAO and sc-PDSI over NEC in 1998–2017. Gray and black dots indicate significant correlations at the 90 and 95% confidence levels

at high latitudes has less influence on the later period of the warm season (Qiao et al. 2020).

NAO is a force that can cause circulation and wave anomalies, especially in winter and summer. For instance, the positive (negative) phase of NAO is favorable for a shallower East Asian trough, which can weaken (strengthen) the East Asian winter monsoon (Feng et al. 2018; Qiao and Feng 2016). Wang et al. (2018) reported that SNAO can affect rainfall anomalies over northern China by altering the thermal forcing of the Tibetan Plateau. Figure 8 shows the spatial correlation distribution of SNAO and sc-PDSI, and

significant positive correlation in NEC indicates that drought events are more likely to occur when SNAO is in negative-phase. Du et al. (2020) demonstrated that negative-phase SNAO could have impacted extreme droughts over northern China. Therefore, the frequency of extreme drought events over NEC may be related to the shift of SNAO to a predominantly negative-phase after 1998.

3.3.2 Atmospheric circulation and wave pattern anomaly associated with extreme droughts

The teleconnection patterns over the North Atlantic–European region and East Asia are shown in Fig. 9. As reported by Watanabe (2004) and Wang et al. (2018), NAO is tied to East Asian climate variability by stationary Rossby waves. Consequently, the influence of sea ice on the SNAO pattern could be one of the pathways leading to extreme droughts over NEC. The regressions of streamfunction against SICI and SSTI (Fig. 9b, d, f, and h) show evident wave trains extending to downstream regions. One of the wave trains originates from North Atlantic–Europe and spreads to central Europe, central Asia, and NEC. Another weakened wave train extends from the Barents–Kara Sea and then propagates eastward and southward to NEC, and this pattern matches the Polar/Eurasia (POL) teleconnection that can influence atmospheric circulation over Eurasia including NEC (Gao et al. 2015). The apparent divergence in the wave activity flux appears at the negative anomaly center of the streamfunction, and it corresponds to the southern center of the SNAO and the Barents–Kara Sea, indicating there are two wave sources although the wave energy dispersion of Barents–Kara Sea is weak. The wave activity flux diverges from the source region along two paths and eventually converges over NEC. As a result, the positive streamfunction anomaly is formed at upper levels over NEC. It could be seen from Fig. 9 that the wave train patterns are also obvious in the middle atmosphere (500 hPa), and eastward shift of the negative-phase SNAO pattern over North
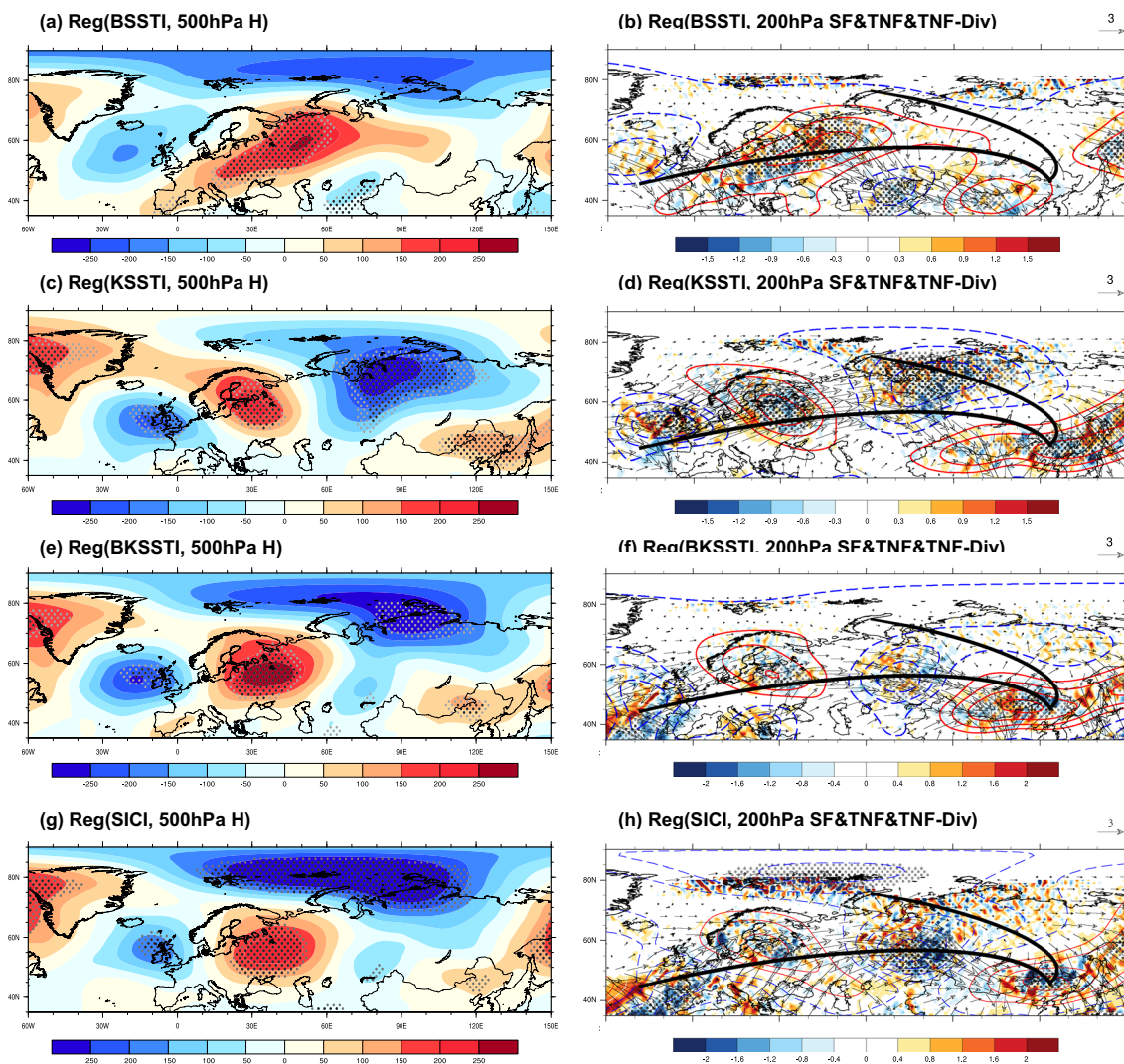
Fig. 9 Regression maps of 1998–2017 with regards to **a**, **b** the BSSTI, **c**, **d** KSSTI, **e**, **f** BKSSTI, **g**, **h** inverted SICI. Left side: geopotential height at 500 hPa; right side: streamfunction (contours; 105 m²/s), TNF (m²/s²) and TNF-Div (m/s²) at 200 hPa. Gray and black dots are the same as in Fig. 4. The black curve is Rossby wave propagate path

Atlantic-Europe region. Under the control of anticyclonic circulation over NEC, extreme drought events are more likely to occur. However, the Barents Sea ice mostly melted in June, and the underlying surface over Barents Sea is the seawater from June to August. It can be seen from regression map that Barents Sea SST contributes to the strengthening of the European ridge (Fig. 9a).

The loss of sea ice signal can last from spring to summer, leading to a large amount of open water over the Barents–Kara Sea. We investigate the possible relationships between decreased sea ice and the atmospheric circulations over NEC. The climate state provides a helpful reference for our discussion of extreme drought. As shown in Fig. 10a, southerly winds from the South China Sea and southwesterly wind influenced by subtropical high prevail over NEC. Correspondingly, the larger quantities of water vapor

(300–1000 hPa) are mainly transported from the South China Sea and western Pacific to NEC (Fig. 10b). The regression circulation maps of summer with regard to inverted SICI and BKSSTI in 1998–2017 are shown in Fig. 10 to clarify the influence of SICI and BKSSTI on extreme droughts over NEC. There is an anomalous anticyclonic center of upper level over NEC (Fig. 10c, d), accompanied by easterly anomalies at 40° N, which decrease the strength of the westerly jet. A positive geopotential height anomaly over NEC at 500 hPa (Fig. 10e, f) and the weakened jet in the upper atmosphere (Fig. 10c), which favors the west extension of subtropical high, can lead to the transport of water vapor to the west. Meanwhile, strong northeasterly winds in low-level winds was not benefit to the northward transport of water vapor (Fig. 10g, h). The draw cross section in Fig. 10j, k indicate that the quasi-barotropic downward motion over

Fig. 10 Climatology of the 850-hPa **a** wind and **b** water vapor flux in August of 1980–2017. Regression circulation maps of summer with regard to inverted SICI and BKSSTI in 1998–2017: **c**, **d** 200 hPa horizontal wind (m/s; vector), **e**, **f** 500 hPa geopotential height (gpm) and horizontal wind (m/s; vector), **g**, **h** 850 hPa horizontal wind (m/s; vector), **i**, **j** integrated water vapor transport (kg/m/s; vector), **k**, **l** vertical–horizontal cross section averaged along 115° E–130° E for vertical wind, **m**, **n** precipitation (mm/day; shaded),. Shadings from light to dark in **c**, **d**, **g**, **h**, **i**, **j** indicate significant regression coefficients at the 90 and 95% confidence levels. Gray and black dots in **e**, **f**, **k**, **l**, **m**, **n** indicate significant correlations at the 90 and 95% confidence levels
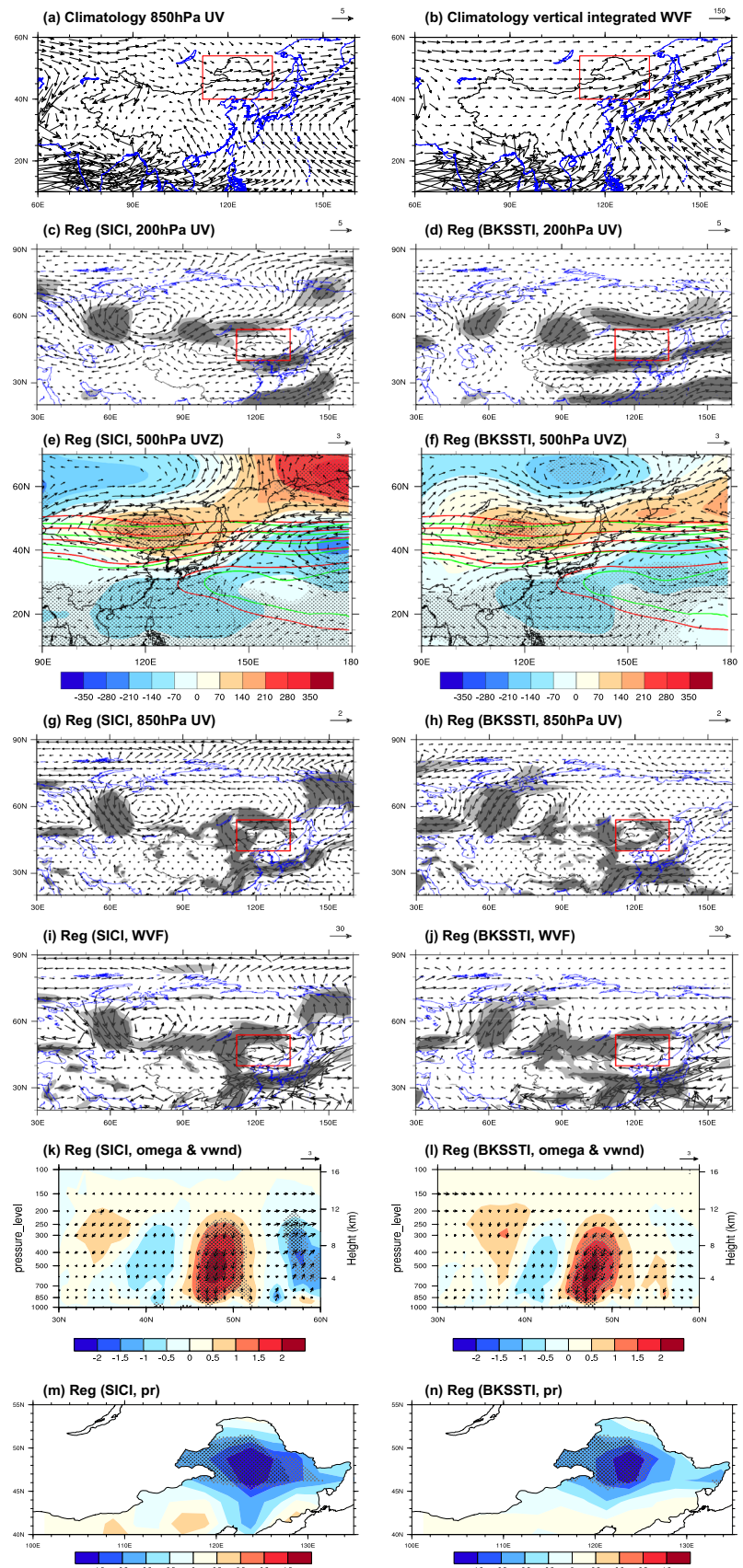
NEC is also significant, which favors the adiabatic heating over NEC. Therefore, this configuration is unfavorable for the convergence of water vapor in NEC (Fig. 10h, j), thereby leading to precipitation deficiency (Fig. 10g, h).

3.4 Model results

To provide more robust evidence for the interpretation of the teleconnection between the reduction in spring sea ice over the Barents Sea and the downstream atmospheric circulation in August, we conduct numerical experiments to examine the atmospheric response to the spring sea ice variability in the Barents Sea. We use the version 5 of Community Atmosphere Model (CAM5) to design two numerical experiments, including a control experiment and a sensitive experiment. The CAM5 has a finite volume grid of $1.9° \times 2.5°$ with 26 hybrid sigma pressure levels. In the control run, the sea ice concentration and SST are prescribed as boundary conditions in the mode, and the other external variables are fixed. In the sensitive run, the sea ice is reduced over Barents–Kara Sea from spring to summer, while other months are prescribed by climatological sea ice, and the boundary condition of SST is set to -1.8 °C where SIC equals zero. The control run and sensitive are both repeated 50 times, with different initial condition, integrated from 1 March to 31 August. We focus on the difference between the sensitivity and control experiments in August to reveal lagged responses to the decreased SIC in spring.

Model-simulated differences in 200 hPa horizontal wind, 500 hPa geopotential height, 850 hPa horizontal wind and precipitation between the sensitive and control experiments are displayed in Fig. 11. The response of 200 hPa winds shows that the NEC and its surroundings affected by significant anomalous anticyclonic, accompanied by easterly anomalies at 42° N, which decrease the strength of the westerly jet (Fig. 11a). The 500 hPa geopotential height is clearly characterized by the two wave trains originating from SNAO and Barents–Kara Sea to NEC, which is similar to the regression maps of geopotential height (Fig. 9g), and the positive geopotential height anomaly and weakened westerly jet over NEC favors the west extension of subtropical high. What's more, strong northeasterly winds in the low-level winds (Fig. 11c), and this was unfavorable for water vapor transportation from south to north under the climatologically typical southwesterly. Duo to the combined influences, it is unfavorable for the convergence of water vapor in NEC (Fig. 11d). Therefore, the anomalous circulation configuration created favorable conditions for extreme drought events over NEC.

4 Summary and discussion

Motivated by extreme droughts over northeast China, which have exhibited a decadal increase since the mid-1990s, this study explored its association with Arctic sea ice loss, as this sea ice has significantly decreased beyond the decadal timescale. The results show the enhanced impact of spring SIC over the Barents Sea on subsequent extreme summer droughts over NEC after 1998, and a possible mechanism
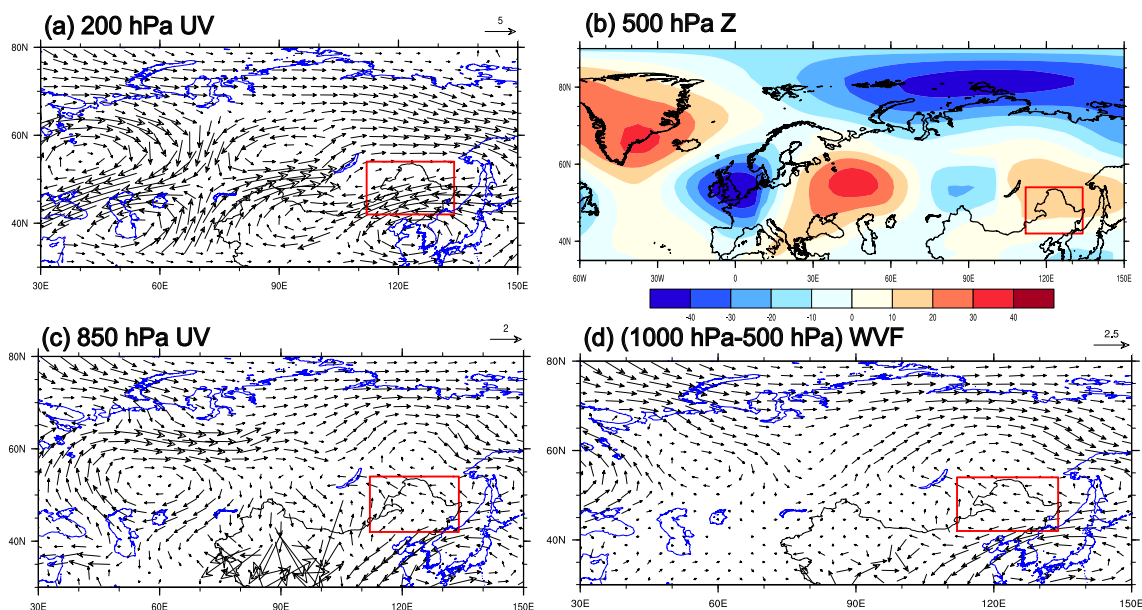

Fig. 11 Composite differences of **a** 200 hPa horizontal wind (m/s; vector), **b** 500 hPa geopotential height (gpm), **c** 850 hPa horizontal wind (m/s; vector) and **d** water vapor flux (WVF kg/m/s; vector) in August between sensitive and control experiments in CAM5

was suggested. The relationship between spring SIC and subsequent extreme summer droughts presented an interdecadal variation, and the correlation coefficients between SICI and sc-PDSI over NEC were − 0.2 and 0.58 for 1979–1998 and 1998–2017, respectively. The reduced spring SIC over the Barents Sea corresponded with positive geopotential height anomalies over NEC during summer. The results indicate that the anomalous anticyclonic circulation patterns and westward subtropical high, which was accompanied by significantly descend motion and less water vapor, led to decreased precipitations and increased droughts.

The spring SIC loss over the Barents enhanced the extreme summer droughts after 1998 largely through two pathways. Sea ice melted into seawater from spring to summer, and the reduced spring SIC memories were sustained by SST during summer. Firstly, the sea ice loss from Barents Sea to Kara Sea results in increased atmospheric baroclinicity over sea ice melting region, and following the initial baroclinic stage of adjustment, the adjustment balance stage was characterized by negative-phase NAO pattern in summer. What's more, the TNF pattern suggested that the wave train originated from SNAO and spread to central Europe, central Asia and NEC. Secondly, another weakened wave train extended from Barents–Kara Sea and then propagated eastward and southward to NEC, similarly to Polar/Eurasia (POL) teleconnection. This associated wave train enhanced the anticyclonic anomaly over NEC, establishing a pronounced link with extreme droughts over NEC.

However, SIC loss is one of the factors that influence extreme drought events over NEC on the decadal timescale. Previous studies have investigated that the variations of precipitation and temperature over NEC is associated with PDO and AMO (Li et al. 2019; Han et al. 2015). Thus, the spring SIC over the Barents Sea could be a driver and potential predictor of extreme droughts over NEC. In this context, extreme drought events over NEC occurred on interdecadal change after 1998, matching the shift of AMO (Zhang et al. 2020a, b). AMO drives the variability in the European climate at decadal timescales (Delworth and Mann 2000; Guan et al. 2019; Knight et al. 2006). Positive-phase AMO caused rapid warming over the North Atlantic, which is responsible for the loss of Arctic sea ice over the Barents Sea (Day et al. 2012). Some studies have verified that AMO modulates the long-term loss of Arctic sea ice and influences summer precipitation over northern Europe (Miles et al. 2014; Screen 2013). In addition, Qian et al. (2014) suggested that AMO affects the decadal variations in summer droughts over eastern China. Zhang et al. (2020a, b) suggested that positive-phase AMO can favor the east extension of negative SNAO. Li et al. (2018) reported that AMO and hot droughts over NEC have a close statistical relationship and are highly correlated with SIC over Barents Sea. Therefore, the interdecadal relation between AMO, SIC over the Barents, and

extreme droughts over NEC should be further investigated in future studies. On the interannual time scale, Li et al. (2018) also have pointed out that SIC in March has close relationship with spring snow cover over Eurasia in April, which further influence the climate over East Asia in early summer. Some studies have proved that snow cover and soil moisture anomalies over Eurasia in spring lead to warm land, which amplifies stationary Rossby waves in summer via memory effects of the land processes (Matsumura et al. 2014; Sato and Nakamura 2019). In addition, Fig. 10e shows the spatial distribution of the 500 hPa geopotential height anomalies related to the inverted SICI is similar to the PJ pattern, indicating that the spring SIC loss over the Barents Sea has a certain modulation effect on the PJ wave train. We further verified that the correlation coefficient between the SICI and PJ pattern index is − 0.45, which is statistically significant at the 99% confidence level. The corresponding mechanisms of SIC over the Barents Sea affecting PJ wave trains on the interannual time scale should also be investigated in future studies.

References

Alexander MA, Bhatt US, Walsh JE, Timlin MS, Miller JS, Scott JD (2004) The atmospheric response to realistic Arctic sea ice anomalies in an AGCM during winter. J Clim 17:890–905

Blüthgen J, Gerdes R, Werner M (2012) Atmospheric response to the extreme Arctic sea ice conditions in 2007. Geophys Res Lett 39:L02707. https://doi.org/10.1029/2011GL050486

Dai A (2011a) Drought under global warming: a review. Wiley Interdiscip. Rev. Clim Change 2:45–65. https://doi.org/10.1002/wcc.81

Dai A (2011b) Characteristics and trends in various forms of the Palmer drought severity index during 1900–2008. J Geophys Res 116:D12115. https://doi.org/10.1029/2010JD015541

Dai A (2013) Increasing drought under global warming in observations and models. Nat Clim Change 3:52–58. https://doi.org/10.1038/NCLIMATE1633

Day JJ, Hargreaves JC, Annan JD, Abe-Ouchi A (2012) Sources of multi-decadal variability in Arctic sea ice extent. Environ Res Lett 7:034011. https://doi.org/10.1088/1748-9326/7/3/034011

Delworth TL, Mann ME (2000) Observed and simulated multidecadal variability in the Northern Hemisphere. Clim Dyn 16:661–676. https://doi.org/10.1007/s003820000075

Deser C, Teng H (2008) Evolution of Arctic sea ice concentration trends and the role of atmospheric circulation forcing, 1979–2007. Geophys Res Lett 35:L02504. https://doi.org/10.1029/2007GL032023

Deser C, Walsh JE, Timlin MS (2000) Arctic sea ice variability in the context of recent atmospheric circulation trends. J Clim 13:617–633

Deser C, Tomas RA, Peng S (2007) The transient atmospheric circulation response to North Atlantic SST and sea ice anomalies. J Clim 20:4751–4767. https://doi.org/10.1175/JCLI4278.1

Dethloff K et al (2006) A dynamical link between the Arctic and the global climate system. Geophys Res Lett 33:L03703. https://doi.org/10.1029/2005GL025245

Du Y, Zhang J, Zhao S, Chen H (2020) Impact of the eastward shift in the negative-phase NAO on extreme drought over northern China in summer. J Geophys Res Atmos 125:e2019JD032019. https://doi.org/10.1029/2019JD032019

Fan K, Xie Z, Wang H, Xu Z, Liu J (2017) Frequency of spring dust weather in North China linked to sea ice variability in the Barents Sea. Clim Dyn. https://doi.org/10.1007/s00382-016-3515-7

Feng G, Zou M, Qiao S (2018) The changing relationship between the December North Atlantic Oscillation and the following February East Asian trough before and after the late 1980s. Clim Dyn 51:4229–4242. https://doi.org/10.1007/s00382-018-4165-8

Ferreira D, Frankignoul C (2005) The transient atmospheric response to midlatitude SST anomalies. J Clim 18:1049–1067

Gao Y et al (2015) Arctic sea ice and Eurasian climate: a review. Adv Atmos Sci 32:92–114. https://doi.org/10.1007/s00376-014-0009-6

Guan X, Ma J, Huang J, Huang R, Zhang L, Ma Z (2019) Impact of oceans on climate change in dry lands. Sci China Earth Sci 62:891–908. https://doi.org/10.1007/s11430-018-9317-8

Guo D, Gao Y, Bethke I, Gong D, Johannessen OM, Wang H (2014) Mechanism on how the spring Arctic sea ice impacts the East Asian summer monsoon. Theor Appl Climatol 115:107–119. https://doi.org/10.1007/s00704-013-0872-6

Han T, Chen H, Wang H (2015) Recent changes in summer precipitation in Northeast China and the background circulation. Int J Climatol 35:4210–4219. https://doi.org/10.1002/joc.4280

Han T, Wang H, Sun J (2017) Strengthened relationship between eastern ENSO and summer precipitation over Northeastern China. J Clim 30:4497–4512. https://doi.org/10.1175/JCLI-D-16-0551.1

He S, Gao Y, Furevik T, Wang H, Li F (2017) Teleconnection between sea ice in the Barents Sea in June and the Silk Road, Pacific–Japan and East Asian rainfall patterns in August. Adv Atmos Sci. https://doi.org/10.1007/s00376-017-7029-y

Hong X, Lu R, Li S (2017) Amplified summer warming in Europe–West Asia and Northeast Asia after the mid-1990s. Environ Res Lett 12(9):094007. https://doi.org/10.1088/1748-9326/aa7909

Huang R, Chen J, Huang G (2007) Characteristics and variations of the East Asian monsoon system and its impacts on climate disasters in China. Adv Atmos Sci 24(6):993–1023. https://doi.org/10.1007/s00376-007-0993-x

Inoue J, Masatake EH, Koutarou T (2012) The role of Barents Sea ice in the wintertime cyclone track and emergence of a warm-Arctic cold-Siberian anomaly. J Clim 25:2561–2568. https://doi.org/10.1175/JCLI-D-11-00449.1

Kim BM, Son SW, Min SK, Jeong JH, Kim SJ, Zhang XD, Shim T, Yoon JH (2014) Weakening of the stratospheric polar vortex by Arctic sea-ice loss. Nat Commun. https://doi.org/10.1038/ncomms5646

Knight JR, Folland CK, Scaife AA (2006) Climate impacts of the Atlantic Multidecadal Oscillation. Geophys Res Lett 33:L17706. https://doi.org/10.1029/2006GL026242

Kushnir Y, Robinson WA, Bladé I, Hall NM, Peng S, Sutton R (2002) Atmospheric GCM response to extratropical SST anomalies: synthesis and evaluation. J Clim 15:2233–2256. https://doi.org/10.1175/1520-0442(2002)015,2233:AGRTES.2.0.CO;2

Li F, Wang H (2013) Autumn sea ice cover, winter Northern Hemisphere annular mode, and winter precipitation in Eurasia. J Clim 26(11):3968–3981

Li H, Chen H, Wang H, Sun J, Ma J (2018) Can Barents Sea ice decline in spring enhance summer hot drought events over northeastern China? J Clim. https://doi.org/10.1175/JCLI-D-17-0429.1

Li J, Zheng F, Sun C et al (2019) Pathways of Influence of the Northern Hemisphere mid-high latitudes on East Asian climate: a review. Adv Atmos Sci 36:902–921. https://doi.org/10.1007/s00376-019-8236-5

Liang L, Li L, Qiang L (2011) Precipitation variability in Northeast China from 1961 to 2008. J Hydrol 404:67–76. https://doi.org/10.1016/j.jhydrol.2011.04.020

Lu R, Oh JH, Kim BJ (2002) A teleconnection pattern in upper-level meridional wind over the North African and Eurasian continent in summer. Tellus A Dyn Meteorol Oceanogr 54(1):44–55. https://doi.org/10.3402/tellusa.v54i1.12122

Ma Z, Fu C (2006) Some evidence of drying trend over northern China from 1951 to 2004. Chin Sci Bull 51(23):2913–2925. https://doi.org/10.1007/s11434-006-2159-0

Matsumura S, Zhang X, Yamazaki K (2014) Summer Arctic atmospheric circulation response to spring Eurasian snow cover and its possible linkage to accelerated sea ice decrease. J Clim 27:6551–6558. https://doi.org/10.1175/JCLI-D-13-00549.1

Miles MW, Divine DV, Furevik T, Jansen E, Moros M, Ogilvie AEJ (2014) A signal of persistent Atlantic multidecadal variability in Arctic sea ice. Geophys Res Lett 41:463–469. https://doi.org/10.1002/2013GL058084

Mori M, Watanabe M, Shigeo H, Inoue J, Kimoto M (2014) Robust Arctic sea-ice influence on the frequent Eurasian cold winters in past decades. Nat Geosci 7:869–873. https://doi.org/10.1038/ngeo2277

Nakamura T, Yamazaki K, Sato T, Ukita J (2019) Memory effects of Eurasian land processes cause enhanced cooling in response to sea ice loss. Nat Commun 10:5111. https://doi.org/10.1038/s41467-019-13124-2

Nitta T (1987) Convective activities in the tropical western Pacific and their impact on the NH summer circulation. J Meteorol Soc Jpn 65(3):373–390. https://doi.org/10.2151/jmsj1965.65.3373

Ogi M, Yamazaki K, Wallace JM (2010) Influence of winter and summer surface wind anomalies on summer Arctic sea ice extent. Geophys Res Lett 37:L07701. https://doi.org/10.1029/2009GL042356

Overland J, Dethloff K, Francis J (2016) Nonlinear response of mid-latitude weather to the changing Arctic. Nat Clim Change 6:992–999. https://doi.org/10.1038/nclimate3121

Pan L (2005) Observed positive feedback between the NAO and the North Atlantic SSTA tripole. Geophys Res Lett 32:L06707. https://doi.org/10.1029/2005GL022427

Petoukhov V, Semenov VA (2010) A link between reduced Barents–Kara sea ice and cold winter extremes over northern continents. J Geophys Res 115:D21111. https://doi.org/10.1029/2009JD013568

Qian C, Yu J, Chen G (2014) Decadal summer drought frequency in China: the increasing influence of the Atlantic Multi-decadal Oscillation. Environ Res Lett 9:12404. https://doi.org/10.1088/1748-9326/9/12/124004

Qiao S, Feng G (2016) Impact of the December North Atlantic Oscillation on the following February East Asian trough. J Geophys Res 121:10074–10088

Qiao S, Zou M, Tang S, Cheung HN, Su H, Li Q, Feng G, Dong W (2020) The enhancement of the impact of the wintertime North Atlantic Oscillation on the subsequent sea surface temperature over the tropical Atlantic since the middle 1990s. J Clim 33:9653–9672. https://doi.org/10.1175/JCLI-D-19-0934.1

Qu X, Huang G (2012) Impacts of tropical Indian Ocean SST on the meridional displacement of East Asian jet in boreal summer. Int J Climatol 32:2073–2080. https://doi.org/10.1002/joc.2378

Rayner NA, Parker DE, Horton EB, Folland CK, Alexander LV, Rowell DP, Kent EC, Kaplan A (2003) Global analyses of sea surface temperature, sea ice, and night marine air temperature since the late nineteenth century. J Geophys Res 108:1063–1082. https://doi.org/10.1029/2002JD002670

Sato T, Nakamura T (2019) Intensification of hot Eurasian summers by climate change and land-atmosphere interaction. Sci Rep 9:10866. https://doi.org/10.1038/s41598-019-47291-5

Screen JA (2013) Influence of Arctic sea ice on European summer precipitation. Environ Res Lett 8:044015. https://doi.org/10.1088/1748-9326/8/4/044015

Shen H, He S, Wang H (2019) Effect of summer Arctic sea ice on the reverse August precipitation anomaly in Eastern China between 1998 and 2016. J Clim 32:3389–3407. https://doi.org/10.1175/JCLI-D-17-0615.1

Shepherd TG (2014) Atmospheric circulation as a source of uncertainty in climate change projections. Nat Geosci 7:703–708

Smith TM, Reynolds RW (2003) Extended reconstruction of global sea surface temperatures based on COADS data (1854–1997). J Clim 16:1495–1510

Sun JQ, Wang H (2012) Changes of the connection between the summer North Atlantic Oscillation and the East Asian summer rainfall. J Geophys Res 117(D8):D08110. https://doi.org/10.1029/2012JD017482

Takaya K, Nakamura H (2001) A formulation of a phase-independent wave activity flux for stationary and migratory quasigeostrophic eddies on a zonally varying basic flow. J Atmos Sci 58(6):608–627

Tang Q, Zhang X, Francis J (2014) Extreme summer weather in northern mid-latitudes linked to a vanishing cryosphere. Nat Clim Change 4:45–50. https://doi.org/10.1038/nclimate2065

Wang M, Overland JE (2009) A sea ice free summer Arctic within 30 years? Geophys Res Lett 36:L07502. https://doi.org/10.1029/2009GL037820

Wang B, Wu ZW, Li JP, Liu J, Chang CP, Ding YH, Wu GX (2008) How to measure the strength of the East Asian summer monsoon. J Clim 17:4449–4463. https://doi.org/10.1175/2008JCLI2183.1

Wang L, Yuan X, Xie Z, Wu P, Li Y (2016) Increasing flash droughts over China during the recent global warming hiatus. Sci Rep 6:30571. https://doi.org/10.1038/srep30571

Wu R, Kirtman BP (2007) Observed relationship of spring and summer east Asian rainfall with winter and spring Eurasian snow. J Clim 20:1285–1304. https://doi.org/10.1175/JCLI4068.1

Wu Z, Zhang P (2015) Interdecadal variability of the mega-ENSO-NAO synchronization in winter. Clim Dyn 45:1117–1128

Wu B, Huang R, Gao D (1999) Effects of variation of winter sea-ice area in Kara and Barents seas on East Asian winter monsoon. Acta Meteorol Sin 13:141–153

Wu B, Zhang R, Wang B (2009a) On the association between spring Arctic sea ice concentration and Chinese summer rainfall: a further study. Adv Atmos Sci 26:666–678. https://doi.org/10.1007/s00376-009-9009-3

Wu Z, Wang B, Li J, Jin F (2009b) An empirical seasonal prediction model of the East Asian summer monsoon using ENSO and NAO. J Geophys Res 114:D18120. https://doi.org/10.1029/2009JD011733

Wu Z, Li X, Li YJ, Li Y (2016) Potential influence of Arctic sea ice to the inter-annual variations of East Asian spring precipitation. J Clim. https://doi.org/10.1175/JCLI-D-15-0128.1

Yang J, Gong D, Wang W, Hu M, Mao R (2012) Extreme drought event of 2009/2010 over southwestern China. Meteorol Atmos Phys 115:173–184. https://doi.org/10.1007/s00703-011-0172-6

Yu M, Li Q, Hayes MJ, Svoboda MD, Heim RR (2014) Are droughts becoming more frequent or severe in China based on the Standardized Precipitation Evapotranspiration Index: 1951–2010? Int J Climatol 34:545–558. https://doi.org/10.1002/joc.3701

Zhang L, Zhou T (2015) Drought over East Asia: a review. J Clim 28(8):3375–3399. https://doi.org/10.1175/JCLI-D-14-00259.1

Zhang Q et al (2009) Drought (in Chinese). China Meteorological Press, Beijing, p 199

Zhang J, Li L, Li D, Deng W (2015) Summer droughts in the north portion of the Yellow River Basin in association with recent Arctic ice loss. Int J Climatol 35(10):2849–2859. https://doi.org/10.1002/joc.4177

Zhang J, Chen H, Zhang Q (2018a) Extreme drought in the recent two decades in northern China resulting from Eurasian warming. Clim Dyn 52(5–6):2885–2902. https://doi.org/10.1007/s00382-018-4312-2

Zhang R, Sun C, Zhang R, Jia L, Li W (2018b) The impact of Arctic sea ice on the inter-annual variations of summer Ural blocking. Int J Climatol 38(12):4632–4650. https://doi.org/10.1002/joc.5731

Zhang J, Chen H, Zhao S (2019) A tripole pattern of summertime rainfall and the teleconnections linking northern China to the Indian subcontinent. J Clim 32(12):3637–3653. https://doi.org/10.1175/JCLI-D-18-0659

Zhang J, Chen Z, Chen H, Ma Q, Teshome A (2020a) North Atlantic multidecadal variability enhancing decadal extratropical extremes in boreal late summer in the early twenty-first century. J Clim 33:6047–6064. https://doi.org/10.1175/JCLI-D-19-0536.1

Zhang R, Sun C, Zhu J, Zhang R, Li W (2020b) Increased European heat waves in recent decades in response to shrinking arctic sea ice and Eurasian snow cover. NPJ Clim Atmos Sci 3(1):7. https://doi.org/10.1038/s41612-020-0110-8

Publisher's Note Springer Nature remains neutral with regard to jurisdictional claims in published maps and institutional affiliations.